How sensitive are physical properties of choline chloride-urea mixtures to composition changes
Molecular dynamics simulations and Kirkwood-Buff theory

Celebi, Alper T.; Dawass, Noura; Moultos, Othonas A.; Vlugt, Thijs J.H.

Citation (APA)
Celebi, A. T., Dawass, N., Moultos, O. A., & Vlugt, T. J. H. (2021). How sensitive are physical properties of choline chloride-urea mixtures to composition changes: Molecular dynamics simulations and Kirkwood-Buff theory. *Journal of Chemical Physics*, *154*(18), Article 184502. https://doi.org/10.1063/5.0049064

Important note
To cite this publication, please use the final published version (if applicable).
Please check the document version above.

The Journal of Chemical Physics

How sensitive are physical properties of choline chloride–urea mixtures to composition changes: Molecular dynamics simulations and Kirkwood–Buff theory

Alper T. Celebi, Noura Dawass, Othonas A. Moultos, and Thijs J. H. Vlugt

COLLECTIONS

Paper published as part of the special topic on Chemical Physics of Deep Eutectic Solvents

View Online   Export Citation   CrossMark

ARTICLES YOU MAY BE INTERESTED IN
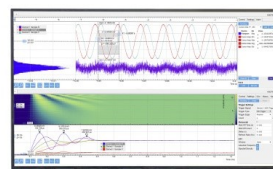
How sensitive are physical properties of choline chloride–urea mixtures to composition changes: Molecular dynamics simulations and Kirkwood–Buff theory

View Online   Export Citation   CrossMark

Alper T. Celebi, [iD] Noura Dawass, [iD] Othonas A. Moultos, [iD] and Thijs J. H. Vlugt[a) [iD]

AFFILIATIONS

Engineering Thermodynamics, Process and Energy Department, Faculty of Mechanical, Maritime, and Materials Engineering, Delft University of Technology, Leeghwaterstraat 39, 2628CB Delft, The Netherlands

Note: This paper is part of the JCP Special Topic on Chemical Physics of Deep Eutectic Solvents.
a)Author to whom correspondence should be addressed: t.j.h.vlugt@tudelft.nl

ABSTRACT

Deep eutectic solvents (DESs) have emerged as a cheaper and greener alternative to conventional organic solvents. Choline chloride (ChCl) mixed with urea at a molar ratio of 1:2 is one of the most common DESs for a wide range of applications such as electrochemistry, material science, and biochemistry. In this study, molecular dynamics simulations are performed to study the effect of urea content on the thermodynamic and transport properties of ChCl and urea mixtures. With increased mole fraction of urea, the number of hydrogen bonds (HBs) between cation–anion and ion–urea decreases, while the number of HBs between urea–urea increases. Radial distribution functions (RDFs) for ChCl–urea and ChCl–ChCl pairs shows a significant decrease as the mole fraction of urea increases. Using the computed RDFs, Kirkwood–Buff Integrals (KBIs) are computed. KBIs show that interactions of urea–urea become stronger, while interactions of urea–ChCl and ChCl–ChCl pairs become slightly weaker with increasing mole fraction of urea. All thermodynamic factors are found larger than one, indicating a non-ideal mixture. Our results also show that self- and collective diffusivities increase, while viscosities decrease with increasing urea content. This is mainly due to the weaker interactions between ions and urea, resulting in enhanced mobilities. Ionic conductivities exhibit a non-monotonic behavior. Up to a mole fraction of 0.5, the ionic conductivities increase with increasing urea content and then reach a plateau.

Published under license by AIP Publishing. https://doi.org/10.1063/5.0049064

I. INTRODUCTION

Deep eutectic solvents (DESs) are a new generation of versatile liquids. DESs are synthesized by mixing a Hydrogen Bond Acceptor (HBA) [e.g., choline chloride (ChCl), tetraoctylammonium chloride] and a Hydrogen Bond Donor (HBD) (e.g., urea, glycerol, decanoic acid).[1,2] DESs are cost-efficient solvents by means of inexpensive starting materials and easy preparation without costly equipment. The final compound usually has a very low vapor pressure and melting point, a large liquid window, non-flammability, biodegradability, biocompatibility, a large electrochemical window, high solubility for different solutes (e.g., CO_2, metal oxides), and

high thermal stability.[1–7] Due to these superior properties, DESs have been considered lately as a promising green alternative to the conventional volatile organic solvents (e.g., benzene, toluene).[5,7,8] In the study by Abbott *et al.*,[9] it was reported for the first time that when ChCl is mixed with urea at a molar ratio of 1:2, it forms a eutectic mixture with a melting point of 12 °C. This mixture, commonly named reline, has become one of the most well-studied DESs.[10] Naturally occurring, biodegradable, inexpensive, and easily accessible starting materials make reline an economically viable, sustainable, and environmentally friendly solvent for a wide range of applications.[1,8] For example, reline is often used for electrocoating and electropolishing of metals.[11–13] Reline has also been used

in extraction and separation, such as CO_2 capture[14,15] and desulfurization of fuels.[16,17] Another use of reline is in the synthesis of functional materials such as nano-structures[18–21] and polymers.[22] In the pharmaceutical industry, mixtures of ChCl and urea were also proposed as an agent in biocatalysis,[23,24] drug solubilization,[25] and biomass treatment.[26]

An accurate control over thermo-physical properties of DESs is essential for the design and optimization of applications mentioned above. Such control can be achieved by tailor-designing the solvents. A simple way to modify the physical properties of DESs is to introduce an additional solute such as water.[27,28] Many experimental[29–35] and computational[27,36–39] studies have shown that the addition of a small amount of water into DESs can significantly change the thermodynamic and transport properties of the mixture. As shown in earlier works by Celebi et al.,[36,39] Shah and Mjalli,[27] Kumari et al.,[40] and Fetisov et al.,[41] the addition of water profoundly alters the molecular structure of reline [i.e., hydrogen bond (HB) network, spatial distributions, orientations, and radial distribution functions (RDFs)]. As a consequence, physical properties such as densities, viscosities, diffusivities, and ionic and thermal conductivities change upon the addition of water. It is important to note that the presence of water is not always desirable, as specific applications may require a moisture-controlled environment.[27] Alternatively, physical properties of DESs can be systematically modified by changing the mixing ratio of starting materials. Changing the mole fraction may significantly affect the thermodynamic and transport properties of DESs such as the melting point. This means that ChCl/urea mixtures are not at the eutectic composition for different mole fractions of urea. Using molecular dynamics (MD) simulations, Sun et al.[42] explored structural characteristics of ChCl and urea mixtures at various urea contents to explore the lowest melting point at the molar ratio 1:2 of ChCl to urea. The authors have shown that with increasing urea content, the number of HBs between choline and chloride significantly decrease, while HBs between urea molecules show an increase. At the molar ratio 1:2 of ChCl to urea, Sun et al.[42] reported shorter HB lifetimes and modest interaction energies between cation–anion, cation–urea, and anion–urea. These microscopic findings were correlated with the lower melting point at this composition. While the relation between the microscopic properties and the melting point of mixtures of ChCl and urea was studied at different molar ratios, the effect of molar composition on many thermodynamic and transport properties of these mixtures remains unknown.

For the prediction of thermodynamic and transport properties of pure fluids and mixtures, molecular simulations and theoretical models can be considered as powerful tools, complementing hard-to-conduct experiments.[43–46] Molecular simulations can be used to correlate microscopic properties of materials with macroscopic behavior. In this regard, the Kirkwood–Buff (KB) theory can be used to connect the microstructure of an isotropic liquid to thermodynamic properties such as thermodynamic factors, partial molar volumes, partial derivatives of the chemical potential with respect to composition, and the isothermal compressibility.[47–49] In the grand-canonical ensemble, thermodynamic quantities are obtained from integrals of RDFs over infinite and open volumes or equivalently from averages of fluctuations in the number of molecules.[47] To compute KB Integrals (KBIs), RDFs can be easily obtained from MD simulations.[50–52] To the best of our knowledge, there are no studies in

the literature focusing on KBIs of DESs from molecular simulations. A very limited number of studies applied the KB theory to Ionic Liquids (ILs). For ILs (i.e., 1-butyl-3-methylimidazolium nitrate), KBIs have been computed from experimental data using the inversion of the KB theory.[53–55] Using MD simulations, Kobayashi et al.[56] computed thermo-physical and structural properties of residual water in dialkylimidazolium-based ILs. Kobayashi et al.[56] compared KBIs computed using molecular simulations with KBIs obtained using experimental data.

KBIs are ideally calculated from infinitely large and open systems. In a larger number of MD studies, KBIs were computed by truncating the infinite integrals to the size of the simulation box.[49] However, truncating to a cutoff distance can result in a poor convergence of KBIs in the thermodynamic limit.[49,57,58] To accurately calculate KBIs using molecular simulation, it is essential to account for system size effects associated with finite and closed systems. Krüger and co-workers[57] derived expressions for KBIs of finite and open subvolumes embedded in a larger reservoir (e.g., simulation box). From the scaling of KBIs of finite subvolumes with their sizes, one can extrapolate to the value at the thermodynamic limit. An advantage of this approach is that the grand-canonical ensemble is accessed while simulating closed systems. This is useful for avoiding molecular insertions and for studying systems where the electro-neutrality condition has to be maintained (e.g., salt solutions, ILs, DESs). When simulating a salt solution in a closed system, it is convenient to treat the mixture as pseudo-binary and consider the cations and anions indistinguishable.[59] In this study, we will show how to compute KBIs and other thermodynamic and transport properties of pseudo-binary mixtures of ChCl and urea.

The main goal of the present work is to investigate the effect of composition on the microscopic structure and thermodynamic and transport properties of ChCl and urea mixtures. To this purpose, MD simulations of eight different mole fractions of urea ranging from 0.20 to 0.71 were performed at 343.15 K and 1 atm. RDFs obtained from equilibrium MD simulations were used to compute KBIs, from which thermodynamic factors and partial molar volumes were calculated. To further explore the effect of microstructure on physical properties of the mixtures, the number of HBs per urea molecule was computed. We also systematically investigated the variations of transport properties such as viscosities, self-diffusivities, Maxwell–Stefan (MS) and Fick diffusivities, and ionic conductivities as a function of the urea mole fraction.

This paper is organized as follows. In Sec. II, we explain how to compute RDFs, KBIs, and collective diffusion of pseudo-binary mixtures. This is followed by the details of the selected force field and MD simulations. In Sec. III, we present and discuss all results for computed densities, RDFs, HBs, KBIs, thermodynamic factors, partial molar volumes, viscosities, self-, Maxwell–Stefan, and Fick diffusivities, and ionic conductivities. Finally, our conclusions are summarized in Sec. IV.

II. MODELS AND METHODS

A. Pseudo-binary systems

ChCl and urea mixtures consist of three components: solvent, cation, and anion. When computing KBIs for finite and closed systems, the electro-neutrality of the system must be maintained.[59]

For this reason, it is convenient to treat the mixture as a pseudo-binary system. In this approach, the cations (choline) and the anions (chloride) are treated as indistinguishable molecules.[57,59]

To obtain KBIs, we first need to compute RDFs of the corresponding pseudo-binary system. For ternary mixtures consisting of species α, θ, and γ, the pseudo-binary system can be described by α and β (where β is either a molecule of type θ or a molecule of type γ). The RDFs of a pseudo-binary system [$g_{\alpha\alpha}(r)$, $g_{\alpha\beta}(r)$, and $g_{\beta\beta}(r)$] are obtained by combining the RDFs of the ternary mixture,

$$g_{\beta\beta}(r) = \frac{N_\theta^2 g_{\theta\theta}(r) + N_\gamma^2 g_{\gamma\gamma}(r) + 2N_\theta N_\gamma g_{\theta\gamma}(r)}{N_\beta^2}, \quad (1)$$

$$g_{\beta\alpha}(r) = \frac{N_\theta g_{\theta\alpha}(r) + N_\gamma g_{\gamma\alpha}(r)}{N_\beta}, \quad (2)$$

where N_i is the number of molecules of species θ, γ, or β. Note that the RDF of the solvent $g_{\alpha\alpha}(r)$ remains unchanged. The derivations of Eqs. (1) and (2) are available in Sec. SII of the supplementary material. To compute KBIs, we will consider open and finite subvolumes embedded in a closed simulation box, as shown in the studies by Krüger and co-workers.[49,51,57,58] For a binary mixture composed of molecules of type α and β, the expression of KBIs of finite subvolumes $G_{\alpha\beta}^V$ is[57]

$$G_{\alpha\beta}^V = \int_0^L \left[g_{\alpha\beta}(r) - 1 \right] 4\pi r^2 w(x) \mathrm{d}r, \quad (3)$$

where L is the size of the subvolume and $w(x)$ is a function that depends on the shape and dimensionality of the subvolume. For a 3D spherical subvolume with diameter L, $w(x) = 1 - 3x/2 + x^3/2$, where $x = r/L$ is the dimensionless distance. Note that KBIs of finite subvolumes $G_{\alpha\beta}^V$ scale with the inverse size of the system,[57,58]

$$G_{\alpha\beta}^V(L) = G_{\alpha\beta}^\infty + \frac{F_{\alpha\beta}^\infty}{L}, \quad (4)$$

where $F_{\alpha\beta}^\infty$ is a term that relates to surface effects of computing KBIs of small subvolumes.[49] By plotting the product of LG^V as a function of L, KBIs in the thermodynamic limit $G_{\alpha\beta}^\infty$ can be obtained from the slope, and the surface term $F_{\alpha\beta}^\infty$ follows from the intercept. Finite-size effects of the computed RDFs are corrected using the method by Ganguly and van der Vegt.[60] From KBIs in the thermodynamic limit, thermodynamic factors and partial molar volumes are computed. In Sec. SIII of the supplementary material, we provide a detailed explanation of how to compute KBIs for binary systems. In addition to the method of Krüger and co-workers[49,51,57,58] and the Ganguly and van der Vegt correction for RDFs,[60] we computed thermodynamic factors using KBIs based on the alternative scaling by Cortes-Huerto and co-workers.[61] In this method, the values of $G_{\alpha\beta}^\infty$ are obtained by the scaling of KBIs of finite subvolumes $G_{\alpha\beta}^V$,

$$G_{\alpha\beta}^V(L, L_{\text{box}}) = G_{\alpha\beta}^\infty \left(1 - \frac{L^3}{L_{\text{box}}^3} \right) + \frac{F_{\alpha\beta}^\infty}{L}, \quad (5)$$

where L_{box} is the length of the simulation box. The reader should note that a RDF correction is already embedded in the scaling shown in Eq. (5).[61] We verified that both scalings yield the same value of the KBI in the thermodynamic limit.

The pseudo-binary description is used to predict the collective diffusion based on the Maxwell–Stefan (MS) and Fick theories. To this purpose, Onsager coefficients (Λ) in a ternary mixture consisting of species α, θ, and γ are computed first. For a pseudo-binary mixture, the value of $\Lambda_{\alpha\alpha}$ is the same as in a ternary mixture. From $\Lambda_{\alpha\alpha}$, MS diffusion coefficients of the pseudo-binary mixture are obtained. Subsequently, Fick diffusion coefficients are computed using MS diffusion coefficients and thermodynamic factors.[62,63] Section SIV of the supplementary material explains all technical details on how to obtain Onsager coefficients and MS and Fick diffusion coefficients for pseudo-binary mixtures. For in-depth discussions about Onsager, MS, and Fick theories, readers are referred to the relevant literature.[50,64–69] To compute the collective diffusivities and properties from KBIs, mole fractions of pseudo-binary mixtures are required, which can be computed from

$$x_\alpha = \frac{N_\alpha}{N_\alpha + N_\theta + N_\gamma} \quad \text{and} \quad x_\beta = 1 - x_\alpha, \quad (6)$$

where α, θ, and γ represent urea molecules, choline cations, and chloride anions in the current study, respectively. β is the indistinguishable molecule representing ChCl, which can be of type θ or γ (i.e., a choline cation or a chloride anion).

B. Force fields

ChCl and urea molecules were modeled using the general amber force field (GAFF).[70] Partial charges were derived using the Restrained Electrostatic Potential (RESP) method based on the Hartree–Fock (HF)/6.31G* level of theory.[71–73] As discussed in the earlier works by Perkins et al.,[72,74] Liu et al.,[75] Shah and Mjalli,[27] and Chaban et al.,[76] charge scaling is essential when simulating ILs and DESs due to overestimated electrostatic interaction potentials. Blazquez and co-workers[77] showed that even for simple electrolytes such as NaCl, charge scaling improves electrostatic interactions. We scaled down the partial charges of ChCl molecules by a factor of 0.8. The GAFF force field combined with reduced charges have been used in MD studies to accurately predict structural, thermodynamic, and transport properties of many ChCl-based DESs such as reline, ethaline, and glyceline.[27,36,37,72,74,78,79] All force field parameters used in this study are listed in Tables SI–SV of the supplementary material.

C. Simulation details

MD simulations were performed using the Large-Scale Atomic/Molecular Massively Parallel Simulator (LAMMPS) version released in August 2018.[80] Eight different mole fractions of urea ranging from 0.20 to 0.71 were considered. For each mole fraction, we considered a small and a large system consisting of 240 and 1200 molecules, respectively. The former was used for computing transport properties (i.e., viscosity, self-diffusivity, and MS diffusion), while the latter was used for computing RDFs required for KBIs. It is important to note that larger system sizes were essential to obtain a sufficiently large linear regime of the scaling of KBIs.[49] Table I shows the number of molecules and the size of the simulation box at each molar ratio of ChCl to urea for all systems simulated in this work.

Initial configurations were generated by randomly inserting molecules in a cubic simulation box using the PACKMOL package.[81] The generated simulation boxes were first relaxed

TABLE I. The mole fractions, number of molecules, and initial box lengths of all simulated systems.

		Small system			Large system		
N_{ChCl}/N_{Urea}	x_{Urea}	N_{ChCl}	N_{Urea}	L_S (Å)	N_{ChCl}	N_{Urea}	L_L (Å)
2/1	0.20	160	80	34.7	800	400	59.4
3/2	0.25	144	96	34.0	720	480	58.1
1/1	0.33	120	120	32.8	600	600	56.2
5/7	0.41	100	140	31.8	500	700	54.4
1/2	0.50	80	160	30.7	400	800	52.6
1/3	0.60	60	180	29.6	300	900	50.6
1/4	0.67	48	192	28.8	240	960	49.3
1/5	0.71	40	200	28.3	200	1000	48.4

using the conjugate gradient method for 10 000 steps. The energy minimization was followed by MD runs in the isothermal–isobaric (*NPT*) ensemble at 343.15 K and 1 atm for 10 ns. In the *NPT* ensemble, average volumes and densities were computed. Starting from the average density obtained from *NPT* runs, each system was then equilibrated at 343.15 K and 1 atm for 1 ns in the canonical (*NVT*) ensemble. Consecutively, transport properties were computed in the next 120 ns. For small systems (see Table I), a 120 ns run typically takes 96 h using 24 CPUs. During production runs, the OCTP (On-the-fly Computation of Transport Properties) plugin in LAMMPS was used to compute transport properties.[82] The OCTP plugin uses Einstein relations combined with the order-*n* algorithm.[43,83] For more details about the OCTP plugin, readers are referred to the original study by Jamali *et al.*[82] Hydrogen bonds were calculated from atomic trajectories using the HBonds plugin in VMD (Visual Molecular Dynamics).[84,85] HBs were computed based on a critical distance of 3.5 Å for heavy-to-heavy atoms and a critical angle of 30° between donor–hydrogen–acceptor.[86,87] RDFs were computed from separate MD simulations of 80 ns of the large systems in the *NPT* ensemble. For large systems (see Table I), a 80 ns run typically takes 720 h using 24 CPUs. Finite-size effects of the reported RDFs are corrected using the method proposed by Ganguly and van der Vegt.[60] Based on the RDFs from *NPT* simulations, KBIs, thermodynamic factors, and partial molar volumes were computed.

All simulations were carried out at 343.15 K and 1 atm. For *NPT* and *NVT* ensembles, temperature and pressure were maintained using the Nosé–Hoover thermostat and barostat with coupling constants of 0.1 ps and 1 ps, respectively.[43] Long range electrostatic interactions between charged species were calculated based on the particle–particle, particle–mesh (pppm) solver with a relative precision of 10^{-6}. The cutoff radius was set to 12 Å for both the Lennard-Jones (LJ) and the real-space part of Coulombic potentials. LJ parameters between the dissimilar species were determined based on the Lorentz–Berthelot mixing rules.[44] Equations of motion were integrated using the Verlet algorithm with a time step of 1 fs. Standard deviations in the transport properties and KBIs were computed based on 10 and 25 independent simulations, respectively. Each independent simulation started from a different initial configuration.

III. RESULTS

In this section, we present our findings on the effect of urea content on the structural, thermodynamic, and transport properties of ChCl and urea mixtures. All raw data and uncertainties are listed in Tables SVI–SXII of the supplementary material.

### A. Densities and structural properties

1. Densities

Densities of ChCl and urea mixtures at 343.15 K and 1 atm are shown in Fig. 1 as a function of the mole fraction of urea [Eq. (6)]. The density of the mixture increases as the mole fraction of urea increases. This trend was expected due to the high density of pure urea. We performed MD simulations of pure ChCl (400 molecules) and pure urea (400 molecules) systems at 343.15 K and 1 atm. The computed density of pure ChCl is 1021.2 kg/m^3, and the density of pure urea is 1453.2 kg/m^3. Values of the densities of mixtures of ChCl and urea are bounded between the densities of the pure components. For a mixture with a molar ratio of 1:2 (x_{Urea} = 0.5), the computed density exhibits an excellent agreement with the density measured experimentally by Yadav and Pandey,[30] showing deviation of less than 1.5%. To the best of our knowledge, experimental data for other mole fractions of urea are not available in the literature.

2. Radial distribution functions

Figure 2 shows RDFs of Ch$^+$, Cl$^-$, and urea molecules at 343.15 K and 1 atm for various mole fractions of urea. The addition of urea to the mixture decreases the intensity of the first RDF peaks for the pairs of Ch$^+$–Ch$^+$, Cl$^-$–Cl$^-$, Ch$^+$–Cl$^-$, and Cl$^-$–urea, as shown in Figs. 2(a)–2(c) and 2(e), respectively. A decrease in the intensity of RDFs peaks indicates weaker affinity between the associated species. A subtle change was obtained for the first peaks of Ch$^+$–urea and urea–urea molecules, as shown in Figs. 2(d) and 2(f). Our results also show that the magnitude of the first RDF peaks of Ch$^+$–Cl$^-$ and Cl$^-$–urea are almost equal, but slightly larger than the peaks for the other remaining pairs. This indicates that anions have stronger interactions with cation and urea. For all molecular pairs,
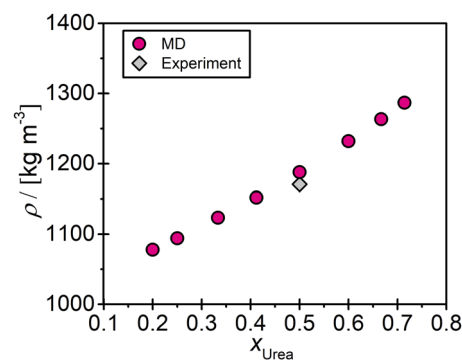
FIG. 1. Computed densities of ChCl/urea mixtures at 343.15 K and 1 atm as a function of the mole fraction of urea. Pink circles represent MD results, and the gray diamond represents experimental data taken from the work of Yadav and Pandey.[30]
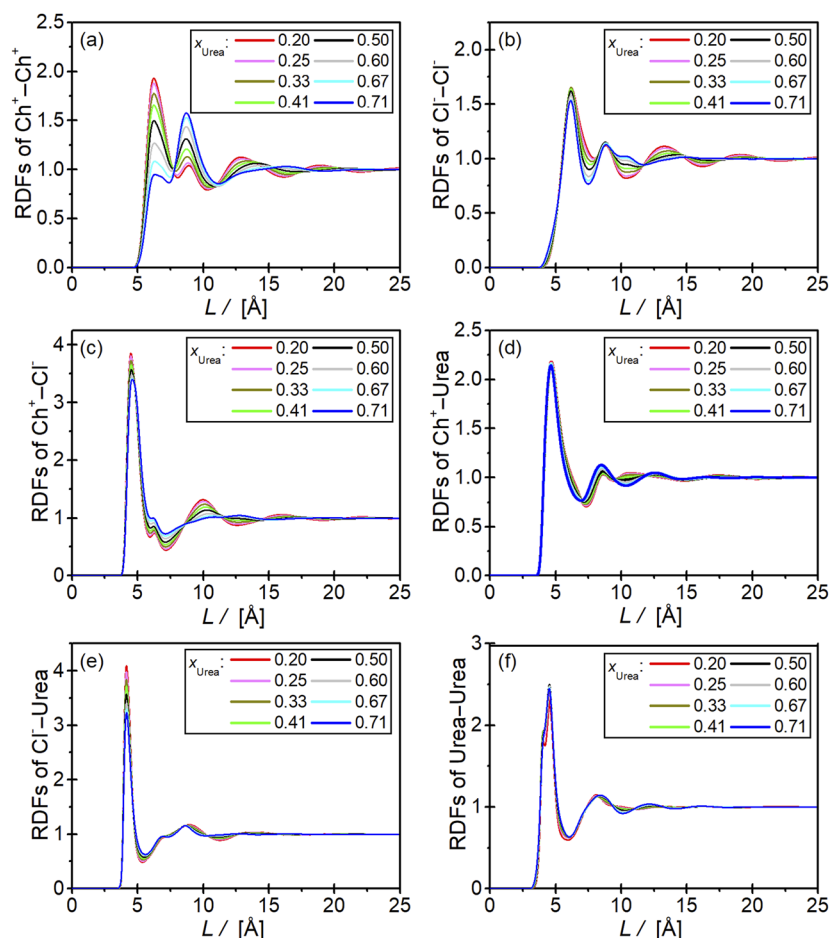
FIG. 2. Radial distribution functions at 343.15 K and 1 atm for (a) Ch^+–Ch^+, (b) Cl^-–Cl^-, (c) Ch^+–Cl^-, (d) Ch^+–urea, (e) Cl^-–urea, and (f) urea–urea for different mole fractions of urea.

the positions of the RDF peaks do not significantly change with the increase in the mole fraction of urea. This illustrates that the variation in the amount of urea has no influence on the packing of the molecules. The first RDF peaks of Cl^-–urea, Ch^+–Cl^-, Ch^+–urea, and Ch^+–Ch^+ are approximately located at distances of 4.1 Å, 4.5 Å, 4.7 Å, and 6.4 Å, respectively. These distances indicate that urea molecules can move between choline cations.[42] This is a sign of well mixing in the solution. The structural asymmetry of the choline cation is probably one of the explanations to why the RDF peaks of Ch^+ are located at larger distances. For the computation of KBIs, Ch^+ cations and Cl^- anions were treated as indistinguishable species as explained in Sec. II A. For this reason, we also computed the RDFs of pseudo-binary ChCl and urea mixtures. These are presented in Fig. S2 of the supplementary material. With increased mole fraction of urea, the intensity of the first peaks of ChCl–ChCl and ChCl–urea pairs slightly decreases, whereas RDFs for urea–urea pairs remain unchanged. These results mainly indicate the weaker interaction of ChCl and urea molecules with respect to the increase in the mole fraction of urea. Similar to the individual RDFs shown in Fig. 2, the locations of the peaks do not significantly change as a function of urea content.

3. Hydrogen bonds

Figure 3 shows the variation of the number of HBs per urea molecule as a function of the mole fraction of urea. With the addition
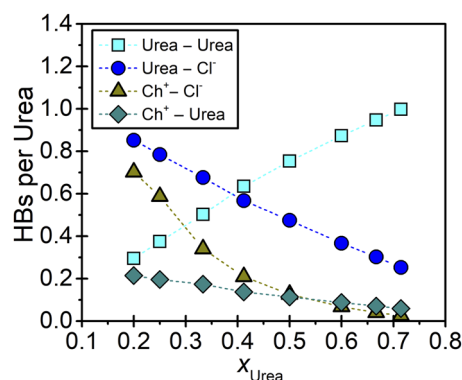
FIG. 3. Hydrogen bonds per urea molecule at 343.15 K and 1 atm as a function of the mole fraction of urea.

of urea to the mixture, HB interactions between urea molecules significantly increase. Adversely, the number of HBs between the pairs of urea–Cl⁻ and Ch⁺–Cl⁻ significantly decreases as the mole fraction of urea increases, while this decrease is less prominent for urea–Ch⁺ pairs. At low mole fractions of urea, HBs are mainly formed between the hydroxyl group in choline and the chloride anion and between nitrogen in urea and the chloride anion. As the mole fraction of urea increases, the contribution of anions decays, and HBs are mainly formed with nitrogen in urea and oxygen in urea. Multiple MD[41,72,88] and experimental[89,90] studies have pointed out that chloride anions strongly contribute to the HB network with the cation and HBD. Other HBs that are formed between different molecules are relatively weaker. The interplay of HBs between ions is critical for explaining the variations of transport and thermodynamic properties.[27] At different mole fractions of urea, the strength of HB interaction varies, and thus, the mobility of the particles changes. As a result, transport properties, such as viscosities, diffusivities, and ionic and thermal conductivities, significantly change. The effect of HBs on the transport properties of different DESs were discussed earlier in the studies by Perkins et al.,[74] Shah and Mjalli,[27] Celebi et al.,[36,39] Baz et al.,[37] and Fetisov et al.[41] The decrease in the number of HBs between ions and the increase in HBs between urea molecules shown in Fig. 3 are important for characterizing the melting point of the DES. Sun et al.[42] pointed out that the decrease in the number of HBs formed by Cl⁻ ions as a function of urea content decreases the melting point of the mixture. The increase in the number of HBs formed between urea molecules results in an increase in the melting point. Therefore, the lowest melting point is achieved at a certain mole fraction for which a reasonable strength of HB interactions for urea and ChCl molecules is established. As shown in Fig. 3, the appropriate mole fraction of urea for HB interactions between ion/urea being maximum and HB interactions between urea molecules being minimum is somewhere between 0.42 and 0.50. It should be noted that the number of HBs is not the only criteria for the eutectic mixture. To further analyze the influence of molecular interactions on the melting point, other quantities such as HB lifetimes and interaction energies for different urea mole factions could be examined.[42]

B. Kirkwood–Buff integrals

In Fig. 4, KBIs in the thermodynamic limit for pairs of urea–urea, ChCl–urea, and ChCl–ChCl at 343.15 K and 1 atm are
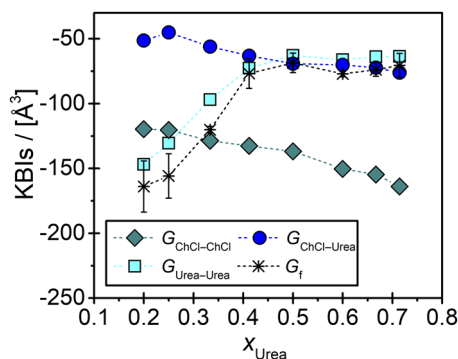

FIG. 4. Kirkwood–Buff integrals for ChCl/urea mixtures at 343.15 K and 1 atm as a function of the mole fraction of urea.

shown as a function of the mole fraction of urea. KBIs of urea–urea pairs are affected the most by the increase in the urea content. Figure 4 shows that the values of $G_{\text{urea–urea}}$ are increasing with the mole fraction of urea. This indicates that urea–urea interactions become stronger as more urea is added to the system. Figure 4 also shows that the values of the KBIs $G_{\text{urea–ChCl}}$ and $G_{\text{ChCl–ChCl}}$ slightly decrease with increasing the content of urea. Consequently, urea–ChCl and ChCl–ChCl interactions become weaker with larger mole fractions of urea. Such trends obtained in KBIs are consistent with the results of RDFs and HBs of urea and ChCl mixtures (see Secs. III A 2 and III A 3).

It is interesting to examine how interactions between dissimilar components (i.e., ChCl–urea) differ from the interactions between similar components (i.e., urea–urea and ChCl–ChCl) at various mole fractions of urea. To study this, the term $G_f = G_{\alpha\alpha} + G_{\beta\beta} - 2G_{\alpha\beta}$ can be used. The G_f is zero for an ideal mixture in which interactions of α and β are equal to the average interactions of molecules of the same type. The term G_f can be computed from integrating the combined RDF $g_f(r) = g_{\alpha\alpha}(r) + g_{\beta\beta}(r) - 2g_{\alpha\beta}(r)$, as shown in Eq. (3). The values of G_f shown in Fig. 4 are computed using this approach. Similar to the KBIs of urea–urea pairs, the values of G_f increase dramatically between $x_{\text{urea}} = 0.25$ and $x_{\text{urea}} = 0.41$. This means that the molecular interactions of the system are shifting for these mole fractions. While the affinity between urea and ChCl is always stronger than the average affinity between similar molecules, attractive interactions between urea and ChCl are stronger when $x_{\text{urea}} < 0.25$. Interestingly, the values of G_f do not significantly change beyond $x_{\text{urea}} = 0.41$ as more urea is added to the system. When studying other microscopic properties of mixtures of ChCl and urea, Sun et al.[42] correlated the change of interactions with the content of urea to the eutectic behavior. The authors reported that the eutectic composition is at a mole ratio 1:2 ChCl and urea.

1. Thermodynamic factors

The so-called thermodynamic factors Γ quantify the non-ideality of a mixture. They are related to derivatives of activity coefficients and thus indicate the phase stability of a mixture.[65,67,91] For a binary mixture consisting of species α and β, the thermodynamic factor (Γ) can be computed from KBIs,[48,49]

$$\Gamma = 1 - \frac{x_\alpha \rho_\beta (G_{\alpha\alpha} + G_{\beta\beta} - 2G_{\alpha\beta})}{1 + \rho_\beta x_\alpha (G_{\alpha\alpha} + G_{\beta\beta} - 2G_{\alpha\beta})} = 1 - \frac{x_\alpha \rho_\beta G_f}{1 + \rho_\beta x_\alpha G_f}, \quad (7)$$

where ρ_α and ρ_β are the average number densities of species α and β. x_α and x_β are the mole fractions of species α and β as defined in Eq. (6) for a pseudo-binary mixture. Thermodynamic factors are directly related to the term G_f. For an ideal mixture, $G_f = 0$, $\Gamma = 1$, and the interactions between α and β are equal to interactions between pairs of the same component. When Γ is positive, the mixture is considered thermodynamically stable, while negative values of Γ correspond to thermodynamically unstable mixtures. The limit $\Gamma \to 0$ indicates de-mixing.
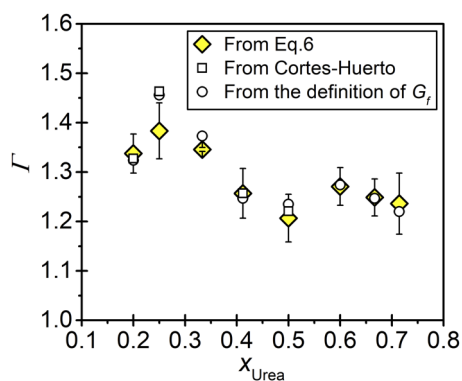
To compute the thermodynamic factors of ChCl and urea mixtures, we use three different descriptions of KBIs: (1) the individual KBIs of $G_{\alpha\alpha}$, $G_{\alpha\beta}$, and $G_{\beta\beta}$ computed by integrating the corresponding RDFs, (2) the term G_f computed by integrating the RDF
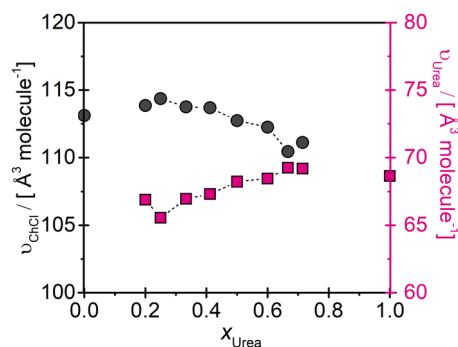
$g_f(r) = g_{\alpha\alpha}(r) + g_{\beta\beta}(r) - 2g_{\alpha\beta}(r)$, and (3) KBIs using the Cortes-Huerto finite-size correction.[61] In the first two approaches, RDFs are corrected for finite-size effects using the method reported by Ganguly and van der Vegt.[60] In the Cortes-Huerto approach, RDFs are corrected using a correction that is independent of the interparticle distance. Based on the computed RDFs, KBIs of finite subvolumes are used to estimate KBIs in the thermodynamic limit ($G_{\alpha\beta}^{\infty}$).[61] This is important to study the effect of the correction method on the computed KBIs and thermodynamic factors. While RDFs are sampled using long and multiple simulations, still, uncertainties of the computed KBIs and the term G_f are not very small (see the supplementary material). Naturally, these uncertainties reflect on the accuracy of the estimation of thermodynamic factors. In Fig. 5, we show the thermodynamic factors of ChCl and urea at $T = 343.15$ K, $P = 1$ atm and various mole fractions of urea. The different methods, used here to compute thermodynamic factors, present very similar results. This could be explained by the fact that large size systems were used to compute KBIs, so finite-size effects were reduced. Figure 5 shows that all of Γ values are found larger than 1 at all urea contents. This indicates that all mixtures of ChCl and urea studied here are not ideal and that the interactions between urea and ChCl are more favorable than interactions between molecules of the same type (i.e., urea–urea and ChCl–ChCl). Computed thermodynamic factors exhibit no distinct trend as a function of the mole fraction of urea. The variations are small, and error bars are large. Although there is no certain trend in Fig. 5, we can see that thermodynamic factors become minimum at a mole fraction of urea of 0.5. This can be attributed to the relatively increased affinity between urea–urea molecules at this mole fraction.

2. Partial molar volumes

The partial molar volume of a component represents the change of volume as a result of the addition of the same component in the mixture at a fixed temperature, pressure, and number of molecules. For binary systems, partial molar volumes can be related to KBIs by[49]

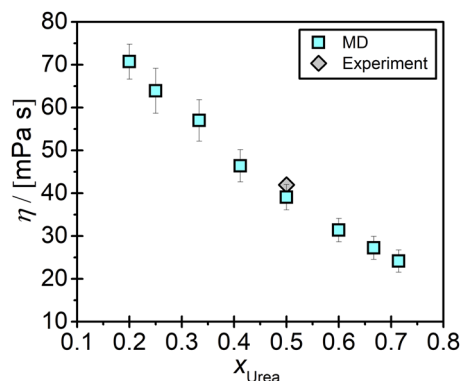**FIG. 6**. Partial molar volumes of ChCl/urea mixtures at 343.15 K and 1 atm as a function of the mole fraction of urea.

$$V_\alpha = \left(\frac{\partial V}{\partial N_\alpha}\right)_{T,P,N_\beta} = \frac{1 + \rho_\beta(G_{\beta\beta} - G_{\alpha\beta})}{\rho_\alpha + \rho_\beta + \rho_\alpha\rho_\beta(G_{\alpha\alpha} + G_{\beta\beta} - 2G_{\alpha\beta})}, \quad (8)$$

where V_α is the partial molar volume of component α. ρ_α and ρ_β are the densities of components α and β, respectively. In Fig. 6, we show the partial molar volumes of urea and ChCl as a function of the mole fraction of urea. As the mole fraction of urea increases, the partial molar volume of urea approaches the molar volume of pure urea. For both components, the change in partial molar volumes with the increasing mole fraction of urea is not significant. This is interesting because the results of HBs, RDFs, and KBIs show that the interactions between urea and ChCl are significantly affected by the change in the urea content. In Fig. 6, we also show the molar volumes of pure urea and pure ChCl, calculated from separate MD simulations of pure systems. Molar volumes for mixtures are consistent with those of pure components.

C. Transport properties

1. Viscosities

Figure 7 shows the computed viscosities of ChCl and urea mixtures at 343.15 K and 1 atm for various mole fractions of urea.

FIG. 5. Thermodynamic factors of ChCl/urea mixtures at 343.15 K and 1 atm as a function of the mole fraction of urea. The yellow diamonds refer to thermodynamic factor computed using Eq. (7). White circles and squares refer to the thermodynamic factors computed using the definition of G_f [obtained by integrating combined RDFs $g_f(r) = g_{\alpha\alpha}(r) + g_{\beta\beta}(r) - 2g_{\alpha\beta}(r)$] and the Cortes-Huerto method.[61]

FIG. 7. Computed viscosities of ChCl/urea mixtures at 343.15 K and 1 atm as a function of the mole fraction of urea. Cyan squares represent MD results, and the gray diamond represents experimental data taken from the work of Yadav and Pandey.[30]

For the mixture of ChCl and urea with a molar ratio of 1:2, MD results are compared with the experimental viscosity measured using a rolling-ball microviscometer by Yadav and Pandey.[30] The computed viscosity is in good agreement with the experimental value, deviating only by 6%. Our MD results show that viscosities of urea and ChCl mixtures decrease linearly with the increase in the mole fraction of urea. This decrease in viscosity is related to the change in the intermolecular interactions. Figure 3 shows that the number of HBs formed by Cl^- anions significantly reduces as the mole fraction of urea increases. As shown in the earlier studies by Kumari et al.,[40] Fetisov et al.,[41] and Hammond et al.,[89] most Cl^- anions are located around the hydroxyl group of the Ch^+ cation, creating an ion pair. Cl^- anions are stabilized by urea molecules in the mixture through hydrogen bonding. The decrease in the number of HBs between Cl^- anions and Ch^+/urea is more dominant compared to the increased number of HBs between urea–urea molecules so that the mobility of the all molecules, including urea, increases. Consequently, all diffusivities (see Sec. III C 2) increase, while viscosities decrease as the urea content in the mixture increases. Such influences of the Cl^- anion on the thermo-physical properties and micro-structural arrangement of the mixture have been shown in earlier neutron diffraction (ND) experiments[89,92] and MD simulations.[40–42] For all mole fractions of urea, the uncertainties of the computed viscosities are found utmost of 9% as shown in Table SVII of the supplementary material.

2. Self-diffusivities

In Fig. 8, the computed self-diffusion coefficients of Ch^+, Cl^-, and urea at 343.15 K and 1 atm are presented as a function of the mole fraction of urea. For all self-diffusion coefficients, computed uncertainties are up to 3%, which is smaller than the marker size. All self-diffusion coefficients are corrected for finite-size effects using the Yeh–Hummer (YH),[50,93]

$$D_{Self}^{\infty} = D_{Self}^{MD} + \frac{k_B T \xi}{6\pi\eta L}, \quad (9)$$

where D_{Self}^{∞} and D_{Self}^{MD} are the finite-size corrected self-diffusion coefficient and self-diffusion coefficient computed in MD simulations, respectively. η is the shear viscosity computed from MD simulations,
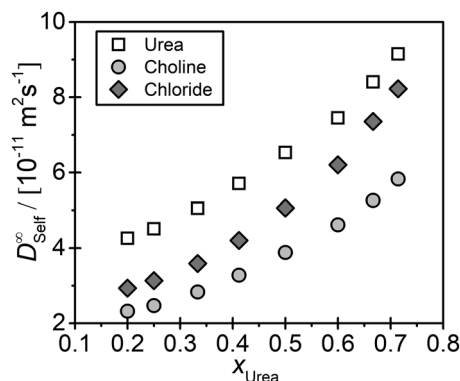
FIG. 8. Finite-size corrected self-diffusion coefficients of Ch^+, Cl^-, and urea molecules at 343.15 K and 1 atm as a function of the mole fraction of urea. The statistical uncertainties can be found in Table SVIII of the supplementary material.

which does not suffer from finite-size effects,[94,95] k_B is the Boltzmann constant, T is the absolute temperature, and ξ is a dimensionless constant equal to 2.837 298 for the periodic (cubic) simulation box. It is important to note that the magnitude of the finite-size correction can significantly change depending on the simulated system and the applied thermodynamic conditions.[50,96] For instance, Moultos et al.[95] showed that the YH correction was found to be ~8% of the self-diffusion coefficients in a system of 250 CO_2 molecules at 323.15 K and 200 bars. The YH correction could be much larger, especially for systems where the size of the solute molecules is significantly larger than the size of the solvent molecules.[50] In the recent study by Erdős et al.,[97] the computed YH correction of self-diffusivities of cyclodextrins in water was found to be as high as ~76% of the final self-diffusion coefficient at 298.15 K and 1 bar. In the current study, the YH corrections computed for systems of ChCl and urea were found to be in the range of 7%–17% of the final self-diffusivities.

Figure 8 shows that all self-diffusion coefficients monotonically increase with the addition of urea to the mixture. This increase is consistent with the decrease in the computed viscosity results, as shown in Fig. 7. As mole fractions of urea increase, the number of HBs between ions and urea/ions and the intensity of RDFs peaks significantly decrease. As a result, molecules can move with a larger mobility and larger diffusion coefficients. Our results also show that the self-diffusion coefficients of urea are always larger than those of Cl^- and Ch^+ ions. Increasing the mole fraction of urea from 0.2 to 0.71 results in 2.8, 2.5, and 2.1 times increase in the self-diffusion coefficients of Cl^-, Ch^+, and urea, respectively. Interestingly, the self-diffusivities of urea molecules increase with the mole fraction of urea, regardless of the increase in the number of HBs formed between pairs of urea–urea. The increase in the self-diffusivities of urea molecules can be attributed to the drop in the number of HBs between pairs of ChCl–urea when more urea is added to the system. In addition to the hydrogen bond formation, self-diffusion coefficients are affected by other factors such as the molecular weight and the hydrodynamic radius.[36]
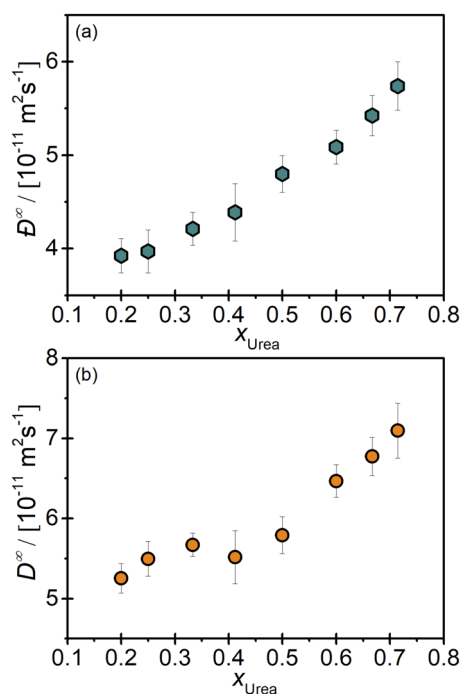
3. Maxwell–Stefan and Fick diffusivities

Similar to self-diffusivities, MS and Fick diffusion coefficients are system size dependent. For MS diffusivities in binary mixtures, Jamali et al.[98,99] developed a finite-size correction on the based on the YH equation [Eq. (9)],

$$Đ^{\infty} = Đ^{MD} + \left(\frac{1}{\Gamma}\right)\frac{k_B T \xi}{6\pi\eta L} = Đ^{MD} + \left(\frac{1}{\Gamma}\right)D^{YH}, \quad (10)$$

where $Đ^{MD}$ and $Đ^{\infty}$ are MS diffusivities obtained from MD simulations and MS diffusivities in the thermodynamic limit, respectively. For binary mixtures, MS diffusion is related to Fick diffusivities via the thermodynamic factor by[98]

$$D^{\infty} = Đ^{\infty}\Gamma, \quad (11)$$

where D^{∞} is the finite-size corrected Fick diffusivity in the binary mixture. In Fig. 9, finite-size corrected MS and Fick diffusion coefficients of pseudo-binary ChCl and urea mixtures at 343.15 K are presented as a function of the mole fraction of urea. Both MS and Fick diffusivities increase with the addition of urea molecules to

FIG. 9. Finite-size corrected (a) Maxwell–Stefan and (b) Fick diffusion coefficients of ChCl/urea mixtures at 343.15 K and 1 atm as a function of the mole fraction of urea.

FIG. 10. Computed ionic conductivities of ChCl/urea mixtures at 343.15 K and 1 atm as a function of the mole fraction of urea. The statistical uncertainties can be found in Table SIX of the supplementary material.
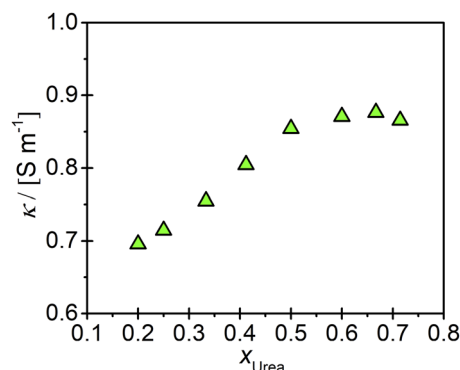
the mixture. This is due to the increased mobilities of individual molecules as explained earlier. Our results also show that MS diffusion coefficients exhibit an increase as a function of urea content. Unlike MS diffusivities, the computed Fick diffusivities exhibit large fluctuations. This is due to the effect of the non-monotonic behavior of the computed thermodynamic factors. The uncertainties of Fick diffusion coefficients are up to 7%, which are considerably larger than those of self-diffusion coefficients.

4. Ionic conductivities

To compute the ionic conductivities of ChCl–urea mixtures in the present work, the Nernst–Einstein (NE) equation was used,[100]

$$\kappa = \frac{e^2}{k_B TV} \sum_i N_i q_i^2 D_{Self,\,i}^{\infty}, \qquad (12)$$

where e is the elementary charge, k_B is the Boltzmann constant, T is the temperature, V is the volume, N_i is the number of molecules of type i, q_i is the charge of the molecule of type i, and $D_{Self,i}^{\infty}$ is the finite-size corrected self-diffusion coefficient of molecules of type i computed from MD simulations. The summation in Eq. (12) only considers Ch^+ and Cl^- ions because urea has no net charge. In Fig. 10, the ionic conductivities of urea and ChCl mixtures at 343.15 K and 1 atm are presented as a function of the mole fraction of urea. Figure 10 shows that, at first, ionic conductivities increase with increasing urea content. For mole fractions larger than 0.5, the ionic conductivities become constant. There is a trade-off between the ionic conductivity and self-diffusivities of charged species. Ionic

conductivities are linearly related to self-diffusivities of ions in the mixture [see Eq. (12)].[31,36,101] As shown in Fig. 10, self-diffusivities of Ch^+ and Cl^- - ions monotonically increase with increasing urea content. Although the increase in self-diffusivities increases the ionic conductivity, it is not the only factor that determines the ionic conductivity. The number density of ions (N_i/V) decreases as a function of the mole fraction of urea. The effect of the reduced ion density balances out the effect of increased self-diffusivities. As a result, ionic conductivities are nearly constant for mole fractions of urea larger than 0.5. It is important to note that ionic conductivities are expected to decrease at higher mole fractions of urea due to a smaller contribution of ions.

IV. CONCLUSIONS

Extensive MD simulations of choline chloride–urea mixtures were performed to investigate the microscopic structure and corresponding thermodynamic and transport properties. HB networks between ions and urea molecules disappear, and the intensity of most RDF peaks decreases as the mole fraction of urea increases. These indicate a considerably weaker intermolecular structure between ChCl and urea molecules. Consequently, a monotonic increase in self-diffusion coefficients and a monotonic decrease in viscosities are obtained. Since the motion of ions and HBDs are less inter-dependent, collective diffusion coefficients thus increase as a function of the urea content. Interestingly, ionic conductivities exhibit a non-monotonic behavior. First, ionic conductivities increase as a function of the mole fraction of urea. Second, for mole fractions of urea larger than 0.5, ionic conductivities do not significantly change. KBIs are used to compute thermodynamic properties such as thermodynamic factors and partial molar volumes. Anions and cations are considered as indistinguishable molecules to accurately compute KBIs in the thermodynamic limit. As the mole fraction of urea increases, KBIs of urea–urea increase, while KBIs of ChCl–ChCl and ChCl–urea pairs slightly decrease. This is connected to the increasing affinity of urea molecules with increasing mole fractions of urea. At all urea contents, thermodynamic factors are larger than one. This indicates that the mixture is not ideal and

the interactions between dissimilar molecules are always more favorable compared to that between similar molecules. The urea content exhibit does not strongly influence the partial molar volumes.

SUPPLEMENTARY MATERIAL

In the supplementary material, we present the force field parameters for ChCl and urea mixtures, tables with raw data for the computed thermo-physical properties, and additional figures. We also provide the derivation for obtaining RDFs of pseudo-binary mixtures, and details on computing KBIs and collective diffusion coefficients for pseudo-binary mixtures.

AUTHORS' CONTRIBUTIONS

A.T.C. and N.D. contributed equally to this work.

ACKNOWLEDGMENTS

DATA AVAILABILITY

The data that support the findings of this study are available from the corresponding author upon reasonable request. The data that support the findings of this study are available within the article and its supplementary material.

REFERENCES

[1] E. L. Smith, A. P. Abbott, and K. S. Ryder, "Deep eutectic solvents (DESs) and their applications," Chem. Rev. **114**, 11060–11082 (2014).

[2] Y. Liu, J. B. Friesen, J. B. McAlpine, D. C. Lankin, S.-N. Chen, and G. F. Pauli, "Natural deep eutectic solvents: Properties, applications, and perspectives," J. Nat. Prod. **81**, 679–690 (2018).

[3] A. P. Abbott, G. Capper, D. L. Davies, K. J. McKenzie, and S. U. Obi, "Solubility of metal oxides in deep eutectic solvents based on choline chloride," J. Chem. Eng. Data **51**, 1280–1282 (2006).

[4] R. B. Leron and M.-H. Li, "Solubility of carbon dioxide in a choline chloride–ethylene glycol based deep eutectic solvent," Thermochim. Acta **551**, 14–19 (2013).

[5] A. Paiva, R. Craveiro, I. Aroso, M. Martins, R. L. Reis, and A. R. C. Duarte, "Natural deep eutectic solvents–solvents for the 21st century," ACS Sustainable Chem. Eng. **2**, 1063–1071 (2014).

[6] L. J. B. M. Kollau, M. Vis, A. van den Bruinhorst, A. C. C. Esteves, and R. Tuinier, "Quantification of the liquid window of deep eutectic solvents," Chem. Commun. **54**, 13351–13354 (2018).

[7] B. B. Hansen, S. Spittle, B. Chen, D. Poe, Y. Zhang, J. M. Klein, A. Horton, L. Adhikari, T. Zelovich, B. W. Doherty *et al.*, "Deep eutectic solvents: A review of fundamentals and applications," Chem. Rev. **121**, 1232–1285 (2021).

[8] Q. Zhang, K. D. O. Vigier, S. Royer, and F. Jérôme, "Deep eutectic solvents: Syntheses, properties and applications," Chem. Soc. Rev. **41**, 7108–7146 (2012).

[9] A. P. Abbott, G. Capper, D. L. Davies, R. K. Rasheed, and V. Tambyrajah, "Novel solvent properties of choline chloride/urea mixtures," Chem. Commun. **2003**, 70–71.

[10] A. P. Abbott, "Model for the conductivity of ionic liquids based on an infinite dilution of holes," ChemPhysChem **6**, 2502–2505 (2005).

[11] A. P. Abbott, A. I. Alhaji, K. S. Ryder, M. Horne, and T. Rodopoulos, "Electrodeposition of copper–tin alloys using deep eutectic solvents," Trans. IMF **94**, 104–113 (2016).

[12] H. Chen, Q. Ye, X. He, J. Ding, Y. Zhang, J. Han, J. Liu, C. Liao, J. Mei, and W. Lau, "Electrodeposited CZTS solar cells from reline electrolyte," Green Chem. **16**, 3841–3845 (2014).

[13] M. Steichen, M. Thomassey, S. Siebentritt, and P. J. Dale, "Controlled electrodeposition of Cu–Ga from a deep eutectic solvent for low cost fabrication of CuGaSe$_2$ thin film solar cells," Phys. Chem. Chem. Phys. **13**, 4292–4302 (2011).

[14] X. Li, M. Hou, B. Han, X. Wang, and L. Zou, "Solubility of CO$_2$ in a choline chloride + urea eutectic mixture," J. Chem. Eng. Data **53**, 548–550 (2008).

[15] G. García, S. Aparicio, R. Ullah, and M. Atilhan, "Deep eutectic solvents: Physicochemical properties and gas separation applications," Energy Fuels **29**, 2616–2644 (2015).

[16] W. Liu, W. Jiang, W. Zhu, W. Zhu, H. Li, T. Guo, W. Zhu, and H. Li, "Oxidative desulfurization of fuels promoted by choline chloride-based deep eutectic solvents," J. Mol. Catal. A: Chem. **424**, 261–268 (2016).

[17] D. V. Wagle, H. Zhao, C. A. Deakyne, and G. A. Baker, "Quantum chemical evaluation of deep eutectic solvents for the extractive desulfurization of fuel," ACS Sustainable Chem. Eng. **6**, 7525–7531 (2018).

[18] D. V. Wagle, H. Zhao, and G. A. Baker, "Deep eutectic solvents: Sustainable media for nanoscale and functional materials," Acc. Chem. Res. **47**, 2299–2308 (2014).

[19] O. S. Hammond, K. J. Edler, D. T. Bowron, and L. Torrente-Murciano, "Deep eutectic-solvothermal synthesis of nanostructured ceria," Nat. Commun. **8**, 14150 (2017).

[20] A. Li, Y. Chen, K. Zhuo, C. Wang, C. Wang, and J. Wang, "Facile and shape-controlled electrochemical synthesis of gold nanocrystals by changing water contents in deep eutectic solvents and their electrocatalytic activity," RSC Adv. **6**, 8786–8790 (2016).

[21] P. Cojocaru, L. Magagnin, E. Gomez, and E. Vallés, "Using deep eutectic solvents to electrodeposit CoSm films and nanowires," Mater. Lett. **65**, 3597–3600 (2011).

[22] D. Carriazo, M. C. Serrano, M. C. Gutiérrez, M. L. Ferrer, and F. del Monte, "Deep-eutectic solvents playing multiple roles in the synthesis of polymers and related materials," Chem. Soc. Rev. **41**, 4996–5014 (2012).

[23] J. T. Gorke, F. Srienc, and R. J. Kazlauskas, "Hydrolase-catalyzed biotransformations in deep eutectic solvents," Chem. Commun. **2008**, 1235–1237.

[24] D. Lindberg, M. de la Fuente Revenga, and M. Widersten, "Deep eutectic solvents (DESs) are viable cosolvents for enzyme-catalyzed epoxide hydrolysis," J. Biotechnol. **147**, 169–171 (2010).

[25] H. G. Morrison, C. C. Sun, and S. Neervannan, "Characterization of thermal behavior of deep eutectic solvents and their potential as drug solubilization vehicles," Int. J. Pharm. **378**, 136–139 (2009).

[26] S. Xia, G. A. Baker, H. Li, S. Ravula, and H. Zhao, "Aqueous ionic liquids and deep eutectic solvents for cellulosic biomass pretreatment and saccharification," RSC Adv. **4**, 10586–10596 (2014).

[27] D. Shah and F. S. Mjalli, "Effect of water on the thermo-physical properties of reline: An experimental and molecular simulation based approach," Phys. Chem. Chem. Phys. **16**, 23900–23907 (2014).

[28] A. Yadav, S. Trivedi, R. Rai, and S. Pandey, "Densities and dynamic viscosities of (choline chloride + glycerol) deep eutectic solvent and its aqueous mixtures in the temperature range (283.15–363.15) K," Fluid Phase Equilib. **367**, 135–142 (2014).

[29] A. Yadav, J. R. Kar, M. Verma, S. Naqvi, and S. Pandey, "Densities of aqueous mixtures of (choline chloride + ethylene glycol) and (choline chloride + malonic acid) deep eutectic solvents in temperature range 283.15–363.15 K," Thermochim. Acta **600**, 95–101 (2015).

[30] A. Yadav and S. Pandey, "Densities and ciscosities of (choline chloride + urea) deep eutectic solvent and its aqueous mixtures in the temperature range 293.15 K to 363.15 K," J. Chem. Eng. Data **59**, 2221–2229 (2014).

[31] V. Agieienko and R. Buchner, "Densities, viscosities, and electrical conductivities of pure anhydrous reline and its mixtures with water in the temperature range (293.15 to 338.15) K," J. Chem. Eng. Data **64**, 4763–4774 (2019).

[32]R. B. Leron and M.-H. Li, "High-pressure density measurements for choline chloride: Urea deep eutectic solvent and its aqueous mixtures at t = (298.15 to 323.15) K and up to 50 MPa," J. Chem. Thermodyn. 54, 293–301 (2012).

[33]H. Shekaari, M. T. Zafarani-Moattar, and B. Mohammadi, "Thermophysical characterization of aqueous deep eutectic solvent (choline chloride/urea) solutions in full ranges of concentration at T = (293.15–323.15) K," J. Mol. Liq. 243, 451–461 (2017).

[34]O. Ciocirlan, O. Iulian, and O. Croitoru, "Effect of temperature on the physico-chemical properties of three ionic liquids containing choline chloride," Rev. Chim. 61, 721–723 (2010).

[35]S. Atashrouz, M. Zarghampour, S. Abdolrahimi, G. Pazuki, and B. Nasernejad, "Estimation of the viscosity of ionic liquids containing binary mixtures based on the Eyring's theory and a modified Gibbs energy model," J. Chem. Eng. Data 59, 3691–3704 (2014).

[36]A. T. Celebi, T. J. H. Vlugt, and O. A. Moultos, "Structural, thermodynamic and transport properties of aqueous reline and ethaline solutions from molecular dynamics simulations," J. Phys. Chem. B 123, 11014–11025 (2019).

[37]J. Baz, C. Held, J. Pleiss, and N. Hansen, "Thermophysical properties of glyceline–water mixtures investigated by molecular modelling," Phys. Chem. Chem. Phys. 21, 6467–6476 (2019).

[38]F. Gabriele, M. Chiarini, R. Germani, M. Tiecco, and N. Spreti, "Effect of water addition on choline chloride/glycol deep eutectic solvents: Characterization of their structural and physicochemical properties," J. Mol. Liq. 291, 111301 (2019).

[39]A. T. Celebi, T. J. H. Vlugt, and O. A. Moultos, "Thermal conductivity of aqueous solutions of reline, ethaline, and glyceline deep eutectic solvents: A molecular dynamics simulation study," Mol. Phys. (published online) (2021).

[40]P. Kumari, Shobhna, S. Kaur, and H. K. Kashyap, "Influence of hydration on the structure of reline deep eutectic solvent: A molecular dynamics study," ACS Omega 3, 15246–15255 (2018).

[41]E. O. Fetisov, D. B. Harwood, I.-F. W. Kuo, S. E. E. Warrag, M. C. Kroon, C. J. Peters, and J. I. Siepmann, "First-principles molecular dynamics study of a deep eutectic solvent: Choline chloride/urea and its mixture with water," J. Phys. Chem. B 122, 1245–1254 (2018).

[42]H. Sun, Y. Li, X. Wu, and G. Li, "Theoretical study on the structures and properties of mixtures of urea and choline chloride," J. Mol. Model. 19, 2433–2441 (2013).

[43]D. Frenkel and B. Smit, Understanding Molecular Simulation: From Algorithms to Applications, 2nd ed. (Elsevier, San Diego, CA, 2001).

[44]M. P. Allen and D. J. Tildesley, Computer Simulation of Liquids, 2nd ed. (Oxford University Press, New York, 2017).

[45]D. C. Rapaport and D. C. R. Rapaport, The Art of Molecular Dynamics Simulation, 2nd ed. (Cambridge University Press, Cambridge, 2004).

[46]G. P. Morriss and D. J. Evans, Statistical Mechanics of Nonequilibrium Liquids, 2nd ed. (ANU Press, Canberra, 2007).

[47]J. G. Kirkwood and F. P. Buff, "The statistical mechanical theory of solutions. I," J. Chem. Phys. 19, 774–777 (1951).

[48]A. Ben-Naim, "Inversion of the Kirkwood-Buff theory of solutions: Application to the water–ethanol system," J. Chem. Phys. 67, 4884–4890 (1977).

[49]N. Dawass, P. Krüger, S. K. Schnell, J.-M. Simon, and T. J. H. Vlugt, "Kirkwood-Buff integrals from molecular simulation," Fluid Phase Equilib. 486, 21–36 (2019).

[50]A. T. Celebi, S. H. Jamali, A. Bardow, T. J. H. Vlugt, and O. A. Moultos, "Finite-size effects of diffusion coefficients computed from molecular dynamics: A review of what we have learned so far," Mol. Simul. (published online) (2021).

[51]N. Dawass, P. Krüger, S. K. Schnell, O. A. Moultos, I. G. Economou, T. J. H. Vlugt, and J.-M. Simon, "Kirkwood–Buff integrals using molecular simulation: Estimation of surface effects," Nanomaterials 10, 771 (2020).

[52]R. Fingerhut, G. Herres, and J. Vrabec, "Thermodynamic factor of quaternary mixtures from Kirkwood-Buff integration," Mol. Phys. 118, e1643046 (2020).

[53]J. E. S. J. Reid, R. J. Gammons, J. M. Slattery, A. J. Walker, and S. Shimizu, "Interactions in water–ionic liquid mixtures: Comparing protic and aprotic systems," J. Phys. Chem. B 121, 599–609 (2017).

[54]S. Heydarian, M. Almasi, and Z. Saadati, "Calculation of Kirkwood-Buff integrals for binary mixtures of 1-butyl-3-methylimidazolium nitrate ionic liquid and alcohols at 298.15 k," J. Mol. Liq. 275, 122–125 (2019).

[55]J. E. S. J. Reid, A. J. Walker, and S. Shimizu, "Residual water in ionic liquids: Clustered or dissociated?," Phys. Chem. Chem. Phys. 17, 14710–14718 (2015).

[56]T. Kobayashi, J. E. S. J. Reid, S. Shimizu, M. Fyta, and J. Smiatek, "The properties of residual water molecules in ionic liquids: A comparison between direct and inverse Kirkwood-Buff approaches," Phys. Chem. Chem. Phys. 19, 18924–18937 (2017).

[57]P. Krüger, S. K. Schnell, D. Bedeaux, S. Kjelstrup, T. J. H. Vlugt, and J.-M. Simon, "Kirkwood–Buff integrals for finite volumes," J. Phys. Chem. Lett. 4, 235–238 (2013).

[58]N. Dawass, P. Krüger, S. K. Schnell, D. Bedeaux, S. Kjelstrup, J. M. Simon, and T. J. H. Vlugt, "Finite-size effects of Kirkwood-Buff integrals from molecular simulations," Mol. Simul. 44, 599–612 (2018).

[59]S. K. Schnell, P. Englebienne, J.-M. Simon, P. Krüger, S. P. Balaji, S. Kjelstrup, D. Bedeaux, A. Bardow, and T. J. H. Vlugt, "How to apply the Kirkwood-Buff theory to individual species in salt solutions," Chem. Phys. Lett. 582, 154–157 (2013).

[60]P. Ganguly and N. F. A. van der Vegt, "Convergence of sampling Kirkwood-Buff integrals of aqueous solutions with molecular dynamics simulations," J. Chem. Theory Comput. 9, 1347–1355 (2013).

[61]R. Cortes-Huerto, K. Kremer, and R. Potestio, "Communication: Kirkwood-Buff integrals in the thermodynamic limit from small-sized molecular dynamics simulations," J. Chem. Phys. 145, 141103 (2016).

[62]X. Liu, S. K. Schnell, J.-M. Simon, D. Bedeaux, S. Kjelstrup, A. Bardow, and T. J. H. Vlugt, "Fick diffusion coefficients of liquid mixtures directly obtained from equilibrium molecular dynamics," J. Phys. Chem. B 115, 12921–12929 (2011).

[63]X. Liu, S. K. Schnell, J.-M. Simon, P. Krüger, D. Bedeaux, S. Kjelstrup, A. Bardow, and T. J. H. Vlugt, "Diffusion coefficients from molecular dynamics simulations in binary and ternary mixtures," Int. J. Thermophys. 34, 1169–1196 (2013).

[64]E. L. Cussler, Multicomponent Diffusion, 1st ed. (Elsevier, Amsterdam, 2013).

[65]R. Taylor and R. Krishna, Multicomponent Mass Transfer, 1st ed. (John Wiley & Sons, 1993), Vol. 2.

[66]E. L. Cussler and E. L. Cussler, Diffusion: Mass Transfer in Fluid Systems, 3rd ed. (Cambridge University Press, Cambridge, 2009).

[67]R. Krishna and J. A. Wesselingh, "The Maxwell-Stefan approach to mass transfer," Chem. Eng. Sci. 52, 861–911 (1997).

[68]R. Krishna and J. M. Van Baten, "Onsager coefficients for binary mixture diffusion in nanopores," Chem. Eng. Sci. 63, 3120–3140 (2008).

[69]X. Liu, A. Martín-Calvo, E. McGarrity, S. K. Schnell, S. Calero, J.-M. Simon, D. Bedeaux, S. Kjelstrup, A. Bardow, and T. J. H. Vlugt, "Fick diffusion coefficients in ternary liquid systems from equilibrium molecular dynamics simulations," Ind. Eng. Chem. Res. 51, 10247–10258 (2012).

[70]J. Wang, R. M. Wolf, J. W. Caldwell, P. A. Kollman, and D. A. Case, "Development and testing of a general amber force field," J. Comput. Chem. 25, 1157–1174 (2004).

[71]C. I. Bayly, P. Cieplak, W. Cornell, and P. A. Kollman, "A well-behaved electrostatic potential based method using charge restraints for deriving atomic charges: The RESP model," J. Phys. Chem. 97, 10269–10280 (1993).

[72]S. L. Perkins, P. Painter, and C. M. Colina, "Molecular dynamic simulations and vibrational analysis of an ionic liquid analogue," J. Phys. Chem. B 117, 10250–10260 (2013).

[73]S. Mainberger, M. Kindlein, F. Bezold, E. Elts, M. Minceva, and H. Briesen, "Deep eutectic solvent formation: A structural view using molecular dynamics simulations with classical force fields," Mol. Phys. 115, 1309–1321 (2017).

[74]S. L. Perkins, P. Painter, and C. M. Colina, "Experimental and computational studies of choline chloride-based deep eutectic solvents," J. Chem. Eng. Data 59, 3652–3662 (2014).

[75]H. Liu, E. Maginn, A. E. Visser, N. J. Bridges, and E. B. Fox, "Thermal and transport properties of six ionic liquids: An experimental and molecular dynamics study," Ind. Eng. Chem. Res. 51, 7242–7254 (2012).

[76]V. V. Chaban, I. V. Voroshylova, and O. N. Kalugin, "A new force field model for the simulation of transport properties of imidazolium-based ionic liquids," Phys. Chem. Chem. Phys. 13, 7910–7920 (2011).

[77] S. Blazquez, I. M. Zeron, M. M. Conde, J. L. F. Abascal, and C. Vega, "Scaled charges at work: Salting out and interfacial tension of methane with electrolyte solutions from computer simulations," Fluid Phase Equilib. **513**, 112548 (2020).

[78] H. S. Salehi, M. Ramdin, O. A. Moultos, and T. J. H. Vlugt, "Computing solubility parameters of deep eutectic solvents from molecular dynamics simulations," Fluid Phase Equilib. **497**, 10–18 (2019).

[79] H. S. Salehi, R. Hens, O. A. Moultos, and T. J. H. Vlugt, "Computation of gas solubilities in choline chloride urea and choline chloride ethylene glycol deep eutectic solvents using Monte Carlo simulations," J. Mol. Liq. **316**, 113729 (2020).

[80] S. Plimpton, "Fast parallel algorithms for short-range molecular dynamics," J. Comput. Phys. **117**, 1–19 (1995).

[81] L. Martínez, R. Andrade, E. G. Birgin, and J. M. Martínez, "PACKMOL: A package for building initial configurations for molecular dynamics simulations," J. Comput. Chem. **30**, 2157–2164 (2009).

[82] S. H. Jamali, L. Wolff, T. M. Becker, M. de Groen, M. Ramdin, R. Hartkamp, A. Bardow, T. J. H. Vlugt, and O. A. Moultos, "OCTP: A tool for on-the-fly calculation of transport properties of fluids with the order-n algorithm in LAMMPS," J. Chem. Inf. Model. **59**, 1290–1294 (2019).

[83] D. Dubbeldam, D. C. Ford, D. E. Ellis, and R. Q. Snurr, "A new perspective on the order-n algorithm for computing correlation functions," Mol. Simul. **35**, 1084–1097 (2009).

[84] W. Humphrey, A. Dalke, and K. Schulten, "VMD: Visual molecular dynamics," J. Mol. Graph. Model. **14**, 33–38 (1996).

[85] M. Kohagen, M. Brehm, Y. Lingscheid, R. Giernoth, J. Sangoro, and F. Kremer, "How hydrogen bonds influence the mobility of imidazolium-based ionic liquids. A combined theoretical and experimental study of 1-n-butyl-3-methylimidazolium bromide," J. Phys. Chem. B **115**, 15280–15288 (2011).

[86] W. Zhao, F. Leroy, B. Heggen, S. Zahn, B. Kirchner, S. Balasubramanian, and F. Müller-Plathe, "Are there stable ion-pairs in room-temperature ionic liquids? Molecular dynamics simulations of 1-n-butyl-3-methylimidazolium hexafluorophosphate," J. Am. Chem. Soc. **131**, 15825–15833 (2009).

[87] A. T. Celebi, M. Barisik, and A. Beskok, "Electric field controlled transport of water in graphene nano-channels," J. Chem. Phys. **147**, 164311 (2017).

[88] E. S. C. Ferreira, I. V. Voroshylova, C. M. Pereira, and M. N. D. S. Cordeiro, "Improved force field model for the deep eutectic solvent ethaline: Reliable physicochemical properties," J. Phys. Chem. B **120**, 10124–10137 (2016).

[89] O. S. Hammond, D. T. Bowron, and K. J. Edler, "Liquid structure of the choline chloride-urea deep eutectic solvent (reline) from neutron diffraction and atomistic modelling," Green Chem. **18**, 2736–2744 (2016).

[90] C. D'Agostino, R. C. Harris, A. P. Abbott, L. F. Gladden, and M. D. Mantle, "Molecular motion and ion diffusion in choline chloride based deep eutectic solvents studied by ^{1}H pulsed field gradient NMR spectroscopy," Phys. Chem. Chem. Phys. **13**, 21383–21391 (2011).

[91] R. Taylor and H. A. Kooijman, "Composition derivatives of activity coefficient models (for the estimation of thermodynamic factors in diffusion)," Chem. Eng. Commun. **102**, 87–106 (1991).

[92] O. S. Hammond, D. T. Bowron, and K. J. Edler, "The effect of water upon deep eutectic solvent nanostructure: An unusual transition from ionic mixture to aqueous solution," Angew. Chem. **56**, 9782–9785 (2017).

[93] I.-C. Yeh and G. Hummer, "System-size dependence of diffusion coefficients and viscosities from molecular dynamics simulations with periodic boundary conditions," J. Phys. Chem. B **108**, 15873–15879 (2004).

[94] S. H. Jamali, R. Hartkamp, C. Bardas, J. Söhl, T. J. H. Vlugt, and O. A. Moultos, "Shear viscosity computed from the finite-size effects of self-diffusivity in equilibrium molecular dynamics," J. Chem. Theory Comput. **14**, 5959–5968 (2018).

[95] O. A. Moultos, Y. Zhang, I. N. Tsimpanogiannis, I. G. Economou, and E. J. Maginn, "System-size corrections for self-diffusion coefficients calculated from molecular dynamics simulations: The case of CO$_2$, N-alkanes, and poly (ethylene glycol) dimethyl ethers," J. Chem. Phys. **145**, 074109 (2016).

[96] I. N. Tsimpanogiannis, O. A. Moultos, L. F. M. Franco, M. B. d. M. Spera, M. Erdős, and I. G. Economou, "Self-diffusion coefficient of bulk and confined water: A critical review of classical molecular simulation studies," Mol. Simul. **45**, 425–453 (2019).

[97] M. Erdős, M. Frangou, T. J. H. Vlugt, and O. A. Moultos, "Diffusivity of α-, β-, γ-cyclodextrin and the inclusion complex of β-cyclodextrin: Ibuprofen in aqueous solutions: A molecular dynamics simulation study," Fluid Phase Equilib. **528**, 112842 (2021).

[98] S. H. Jamali, L. Wolff, T. M. Becker, A. Bardow, T. J. H. Vlugt, and O. A. Moultos, "Finite-size effects of binary mutual diffusion coefficients from molecular dynamics," J. Chem. Theory Comput. **14**, 2667–2677 (2018).

[99] S. H. Jamali, A. Bardow, T. J. H. Vlugt, and O. A. Moultos, "Generalized form for finite-size corrections in mutual diffusion coefficients of multicomponent mixtures obtained from equilibrium molecular dynamics simulation," J. Chem. Theory Comput. **16**, 3799–3806 (2020).

[100] M. T. Humbert, Y. Zhang, and E. J. Maginn, "PyLAT: Python LAMMPS analysis tools," J. Chem. Inf. Model. **59**, 1301–1305 (2019).

[101] F. S. Mjalli and O. U. Ahmed, "Physical properties and intermolecular interaction of eutectic solvents binary mixtures: Reline and ethaline," Asia-Pac. J. Chem. Eng. **11**, 549–557 (2016).